



Cite this: *Nanoscale*, 2015, **7**, 16046

Synthesis of in-plane and stacked graphene/hexagonal boron nitride heterostructures by combining with ion beam sputtering deposition and chemical vapor deposition†

Jun Hua Meng,^a Xing Wang Zhang,^{*a} Hao Lin Wang,^a Xi Biao Ren,^b Chuan Hong Jin,^b Zhi Gang Yin,^a Xin Liu^a and Heng Liu^a

Graphene/hexagonal boron nitride (h-BN) heterostructures have attracted a great deal of attention in recent years due to their unique and complementary properties for use in a wide range of potential applications. However, it still remains a challenge to synthesize large-area high quality samples by a scalable growth method. In this work, we present the synthesis of both in-plane and stacked graphene/h-BN heterostructures on Cu foils by sequentially depositing h-BN via ion beam sputtering deposition (IBSD) and graphene with chemical vapor deposition (CVD). Due to a significant difference in the growth rate of graphene on h-BN and Cu, the in-plane graphene/h-BN heterostructures were rapidly formed on h-BN domain/Cu substrates. The large-area vertically stacked graphene/h-BN heterostructures were obtained by using the continuous h-BN film as a substrate. Furthermore, the well-designed sub-bilayered h-BN substrates provide direct evidence that the monolayered h-BN on Cu exhibits higher catalytic activity than the bilayered h-BN on Cu. The growth method applied here may have great potential in the scalable preparation of large-area high-quality graphene/h-BN heterostructures.

Received 6th July 2015,
Accepted 20th August 2015

DOI: 10.1039/c5nr04490a

www.rsc.org/nanoscale

Introduction

Two-dimensional (2D) graphene has attracted a great deal of attention in recent years due to its unique band structure, electronic properties, as well as its potential applications in nanoelectronics. Hexagonal boron nitride (h-BN), an isomorph of graphene with a very close lattice constant, self-terminating surface, chemical inertness, and a band gap of 5.9 eV, is considered to be an ideal candidate for integration with graphene.^{1–6} Recently, various graphene/h-BN heterostructures have been investigated theoretically and experimentally, in the interest of combining their complementary properties for use in a wide range of applications. On the one hand, owing to their relatively small lattice mismatch (1.7%) and the same crystal structure, graphene and h-BN can be merged into a

single atomic layer, leading to the formation of in-plane graphene/h-BN heterostructures with promising electronic applications.^{7–9} On the other hand, the close lattice match with graphene, along with its atomically flat and dangling-bond-free surface, makes h-BN a suitable dielectric substrate for graphene-based devices. Indeed, an order of magnitude improvement in carrier mobility,¹⁰ micrometer scale ballistic transport¹¹ and quantum Hall effect^{12,13} have been observed in the stacked graphene/h-BN heterostructures.

Despite the great interest in graphene/h-BN heterostructures, there has been very limited experimental success in achieving these structures. The chemical vapor deposition (CVD) technique is expected to be a promising approach to obtain these hybrid material systems. Ci *et al.* firstly reported the synthesis of large-area atomic layers of randomly distributed graphene and h-BN domains by CVD using a mixed carbon and ammonia borane source.⁷ Furthermore, shape-controlled in-plane graphene/h-BN heterostructures were prepared by an etching-regrowth procedure,^{14,15} meanwhile the epitaxial growth of h-BN on the edge of graphene gave rise to a well stitched clean interface.^{16,17} For the vertically stacked heterostructures, the epitaxial growth of graphene on exfoliated h-BN flakes has been reported as well.^{13,18} However, these samples are only suitable for atomic scale characterization of the interface structures, but are not feasible for scalable fabrication.

^aKey Lab of Semiconductor Materials Science, Institute of Semiconductors, Chinese Academy of Sciences, Beijing, 100083, P. R. China. E-mail: xwzhang@semi.ac.cn

^bState Key Laboratory of Silicon Materials, and Department of Materials Science and Engineering, Zhejiang University, Hangzhou, 310027, P. R. China

† Electronic supplementary information (ESI) available: SEM images of the h-BN domains on Cu foils; AFM image of h-BN domains transferred onto SiO₂/Si; SEM image of the continuous monolayered h-BN film; HRTEM images for the stacked graphene/h-BN heterostructures with different Moiré patterns; XPS core level spectra of Cu 2p, C 1s, and N 1s for the 12 min grown graphene/h-BN film. See DOI: 10.1039/c5nr04490a

Recently, the synthesis of large-area vertically stacked films was realized by direct growth of h-BN and graphene *via* a two-step CVD process.^{19,20} In contrast, both discrete graphene and h-BN flakes patched as well as stacked together were obtained by using the same Cu substrate but growing the two materials separately under CVD.²¹ More recently, Gao *et al.* developed the selective growth of in-plane and stacked graphene/h-BN heterostructures on Cu foils through a temperature-triggered switching reaction.²² Although significant efforts have been devoted to the graphene/h-BN hybrid structures, it still remains a challenge to synthesize large-area high quality samples by a scalable growth method. Besides, a systematic investigation on the direct growth of graphene on h-BN domains or h-BN films with different layers is also highly desirable for elucidating the mechanism of graphene nucleation on h-BN.

In this work, we present the synthesis of both in-plane and stacked graphene/h-BN heterostructures on Cu foils by sequentially depositing h-BN *via* ion beam sputtering deposition (IBSD) and graphene with CVD. Due to a significant difference in the growth rate of graphene on h-BN and Cu, the in-plane graphene/h-BN heterostructures were rapidly formed after 30 s growth of graphene on h-BN domain/Cu substrates. By increasing the growth time, a continuous graphene film was grown on the h-BN domains, resulting in a graphene/h-BN hybrid film. On the other hand, the large-area stacked graphene/h-BN heterostructures were obtained by using sequential CVD growth of single-layer graphene directly onto an IBSD-grown h-BN film on Cu. Moreover, the well-designed sub-bilayered h-BN allows us to clearly elucidate the effect of the layer number of h-BN on the growth of graphene. The growth method applied here may open up new avenues for the controllable growth of large-area high-quality graphene/h-BN heterostructures.

Experimental section

Preparation of h-BN domains and films on Cu foils

The h-BN was prepared by IBSD at 1050 °C, and the detailed procedure has been described in our previous report.²³ For the growth process, a cleaned Cu foil (99.8% purity, 25 µm thickness, Alfa Asear) was firstly annealed at 1050 °C for 20 min under a 20 sccm (standard cubic centimeters per minute) H₂ atmosphere. Then, boron and nitrogen species were sputtered from a pure h-BN target by the Ar ion beam (1.0 keV), resulting in the growth of h-BN on the Cu foils. After growth, the samples were cooled down to room temperature under an Ar atmosphere quickly. By controlling the growth time to 3 min and 15 min, separated h-BN domains on Cu or a sub-bilayered h-BN film can be obtained.

Growth of graphene/h-BN heterostructures

The pre-grown h-BN/Cu substrates were loaded into a CVD system for the growth of graphene. To avoid the H₂ etching effect, the growth chamber was heated up to 1000 °C at a pressure of 0.1 Pa without introducing any gas. When the

temperature reached 1000 °C, a mixture gas of Ar (50 sccm) and CH₄/H₂ (5 sccm, the flow ratio of 1 : 2) was introduced into the chamber to grow graphene. The chamber pressure was maintained at a constant pressure (2 kPa) during growth and the growth time was varied from 20 s to 12 min. After growth, both CH₄/H₂ and Ar were turned off and the growth chamber was cooled down to room temperature. The growth protocol is illustrated in Fig. S1.† The heterostructures were transferred onto different substrates for characterization with the same method for graphene. The as-grown samples were spin-coated with poly(methyl methacrylate) (PMMA) on the surface as a supportive layer. After completely etching the Cu foils with the FeCl₃ solution, the films were transferred onto the SiO₂/Si or quartz substrate. Then, the PMMA layers were dissolved in acetone to yield graphene/h-BN heterostructures.

Characterization

The surface morphologies of the samples were investigated by scanning electron microscopy (SEM, FEI Quanta-450) and optical microscopy (Olympus MX51). Tapping mode atomic force microscopy (AFM, NTMDT Solver P47) was used to obtain the phase images. Raman spectra were acquired with a Renishaw InVia-Reflex spectrometer using a 532 nm laser as the excitation source. Optical absorption spectra of the samples were recorded by using a Varian Cary 5000 UV-Vis spectrophotometer in a double-beam mode. High-resolution transmission electron microscopy (HRTEM, Titan G2 60-300 FEI, operated at 80 kV) was employed for structural analysis of the samples. X-ray photoelectron spectroscopy (XPS) measurements were performed on an AXIS-Ultra instrument with a monochromated Al K α source (1486.68 eV).

Results and discussion

Fig. 1 illustrates the growth strategy of in-plane and stacked graphene/h-BN heterostructures. High-quality large-area h-BN domains and films were firstly grown on Cu foils by the optimized IBSD method, and the experimental details can be found in our previous report.²³ The Cu foils partially covered with the h-BN domains were used as the substrates for the

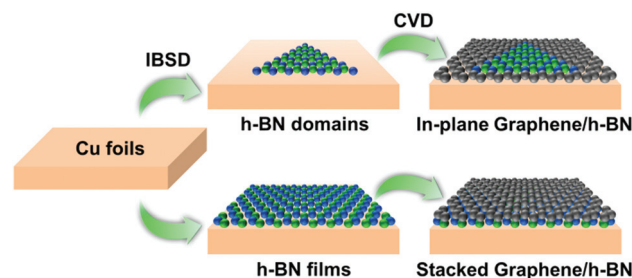


Fig. 1 Schematic illustration of the growth of graphene/h-BN heterostructures by combining with IBSD and CVD. The h-BN domains and continuous h-BN films were used as the substrates for the growth of in-plane and stacked graphene/h-BN heterostructures, respectively.

growth of in-plane graphene/h-BN heterostructures. To synthesize the stacked graphene/h-BN heterostructures, a continuous h-BN film was firstly grown on a Cu foil by IBSD, then immediately followed by the graphene growth with CVD. To avoid the H₂ etching effect,^{21,24} the pre-grown h-BN was heated to the growth temperature (1000 °C) under a pressure of 0.1 Pa (without introducing any gas), and then the CVD growth of graphene was conducted with a low H₂/CH₄ flow rate ratio of 2 : 1.

A typical SEM image of the pre-grown h-BN domains on Cu foils is shown in Fig. 2a, in which the characteristic triangular h-BN domains with their sides parallel to each other are frequently observed. Similar to the CVD-grown graphene,^{25,26} the self-aligned h-BN domains were formed on the melted/resolidified Cu surface, while the randomly oriented h-BN grains were observed on the un-melted Cu substrate (Fig. S2†). In addition, the monolayered nature of the pre-grown h-BN was confirmed by AFM height analysis after the sample was transferred onto SiO₂/Si (Fig. S3†). Fig. 2b–e shows the SEM images of graphene grown on h-BN domains with the growth times of 20, 30, 60 and 90 s, respectively. It can be clearly seen that triangular

h-BN domains with light colour are in contrast to the irregular graphene flakes with dark colour, as is commonly reported.^{21,22} Additionally, the sizes of h-BN domains are almost unchanged, indicating that the H₂ etching effect for h-BN is negligible during the graphene growth. At the initial growth stage of 20 s, the graphene flakes nucleated randomly on the bare surface of Cu foils, as shown in Fig. 2b. This is different from the h-BN growth on graphene grains, in which the h-BN was preferentially grown from the edge of graphene.^{16,17,21,27} Given the growth time of 30 s, the growing graphene was perfectly filled in the region between h-BN domains, forming in-plane graphene/h-BN heterostructures on the whole Cu foils (Fig. 2c). The formation of in-plane heterostructures is also confirmed by the optical image of the sample transferred onto a SiO₂/Si substrate (Fig. 2f). In general, the optical contrast of monolayered h-BN on 300 nm SiO₂/Si is very small,²⁸ while a remarkable contrast in photography is usually used to distinguish graphene from the SiO₂/Si substrate. Here, the triangular h-BN domains (light colour) embedded in the percolating graphene film (dark colour) can be clearly identified from the inset of Fig. 2f. By further increasing the growth time to 60 s, the graphene flakes extended on top of the nearby h-BN domains (Fig. 2d). The underlying triangular h-BN domains can be readily distinguished, as highlighted in Fig. 2d by the white dashed lines, providing direct evidence that both in-plane and stacked graphene/h-BN heterostructures were obtained on Cu foils. After 90 s growth, the graphene flakes coalesced into a continuous film on the pre-grown h-BN domains, forming a graphene/h-BN hybrid film (Fig. 2e). Additionally, a few wrinkles can also be observed in Fig. 2e, which arise from the differential thermal expansion of graphene compared to the Cu substrate.

The phase image of AFM has been employed recently to distinguish graphene and h-BN in an in-plane and patched heterostructure.^{16,21} Fig. 3a–c shows the representative AFM phase images for the samples with the growth times of 30, 60, and 90 s after being transferred onto 300 nm SiO₂/Si substrates, respectively. Similar to the above SEM images, the embedded triangular h-BN domains can be clearly distinguished from the surrounding graphene (Fig. 3a), while the overlapped regions between graphene and h-BN can be easily identified for the 60 s sample, as highlighted by the blue dashed circle in Fig. 3b. For the graphene/h-BN hybrid film, the overall contrast of the phase image is rather uniform except for a few wrinkles, demonstrating that a continuous graphene layer was formed (Fig. 3c). Thus, the AFM phase images confirm the patching nature of the in-plane graphene/h-BN heterostructures, which is in good agreement with the SEM results in Fig. 2.

To confirm that graphene could indeed be grown on h-BN domains, we collected Raman spectra on the pre-grown h-BN domains, reference graphene, and 30 s-grown graphene/h-BN heterostructure after the samples were transferred onto SiO₂/Si substrates, as shown in Fig. 3d. The pre-grown h-BN domains show one dominant peak at 1367 cm⁻¹ due to the E_{2g} vibrational mode of h-BN (the inset of Fig. 3d).²⁸ After CVD growth, the two characteristic peaks of graphene G and 2D

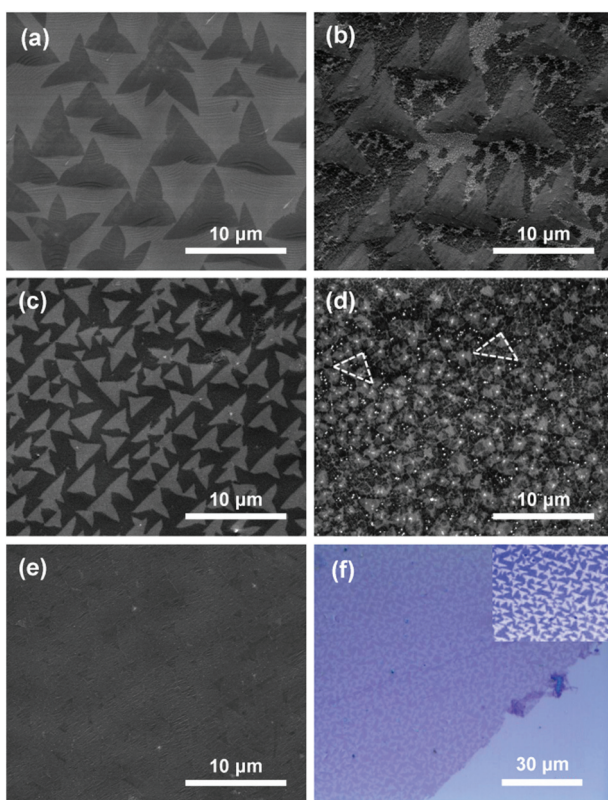


Fig. 2 Characterization of in-plane graphene/h-BN heterostructures. (a) SEM image of the pre-grown h-BN domains on Cu foils. (b–e) SEM images of graphene grown on h-BN domains with the growth times of (b) 20, (c) 30, (d) 60, and (e) 90 s. The underlying triangular h-BN domains in (d) can be readily distinguished, as highlighted by the white dashed lines. (f) Optical micrograph of the 30 s grown sample transferred onto a SiO₂/Si substrate. The inset in (f) reveals that the triangular h-BN domains (lighter colour) are embedded in the percolating graphene film (darker colour).

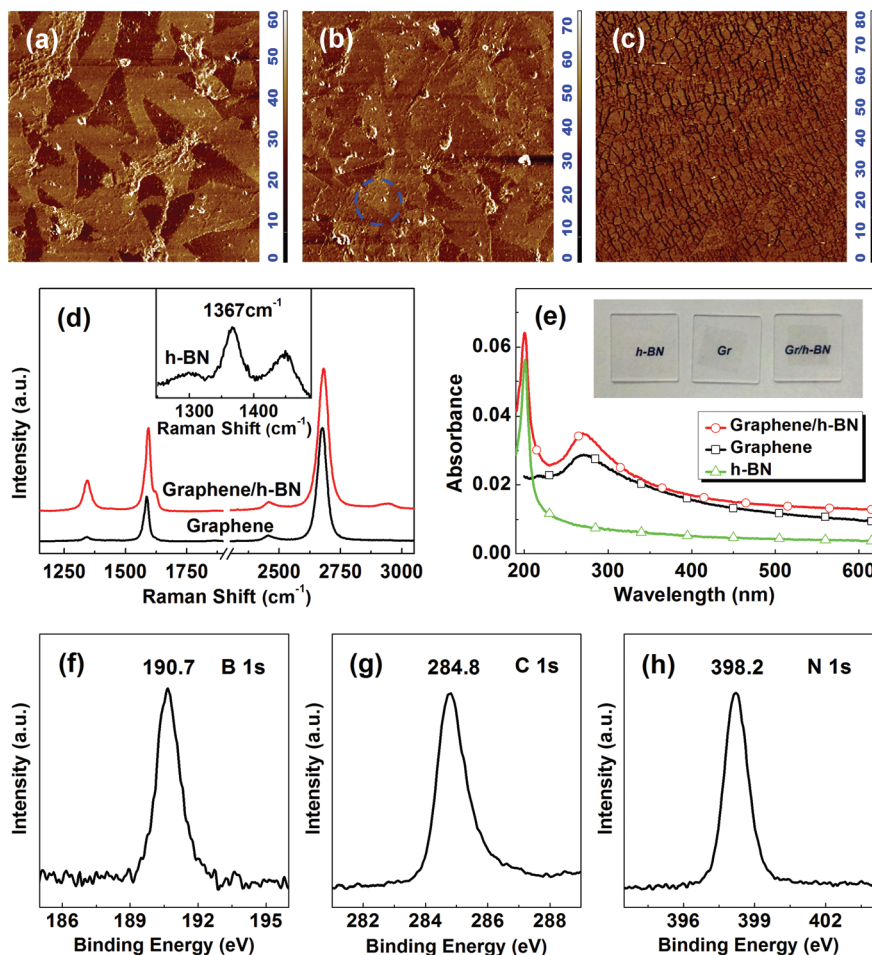


Fig. 3 (a–c) AFM phase images for the samples with the growth time of (a) 30, (b) 60, and (c) 90 s after being transferred onto 300 nm SiO₂/Si substrates. The blue dashed circle in (b) shows the overlapped regions between graphene and h-BN. The scan area in (a–c) is 10 μm × 10 μm. (d) Raman spectra of the in-plane graphene/h-BN heterostructure and the reference graphene synthesized directly on Cu. The inset shows the Raman spectrum of the pre-grown h-BN domains. (e) UV-Vis absorption spectra of the pre-grown h-BN domains, the reference graphene, and the graphene/h-BN hybrid film transferred onto quartz substrates. Their photographs shown in the inset demonstrate different transparencies for these samples. (f–h) XPS spectra of the graphene/h-BN heterostructures showing (f) B 1s, (g) C 1s and (h) N 1s core-level peaks.

bands at 1593 and 2681 cm⁻¹ show that graphene was indeed grown on the h-BN. The sharp and symmetric 2D peaks with a peak intensity ratio of $I_{2D}/I_G > 1.5$ are characteristic of single-layer graphene, which is similar to the reference graphene. However, an obvious D peak around 1350 cm⁻¹ was detected from the graphene/h-BN sample, indicating the presence of a few defects in graphene. Furthermore, because of the proximity of the strong D peak of graphene (1350 cm⁻¹) to the much weaker characteristic peak of h-BN (1367 cm⁻¹),¹⁶ it is not possible to resolve the h-BN signal from the strong D peak of graphene.

To confirm that the h-BN domains are still remaining even after CVD growth of graphene, the UV-Vis absorption spectrum was measured for the graphene/h-BN hybrid film transferred onto a quartz substrate, as shown in Fig. 3e. For comparison, the UV-Vis spectra of the reference monolayer graphene and h-BN are also included in Fig. 3e. An absorption peak at about

200 nm corresponds to the π–π* interband transition of h-BN,³ whereas a peak around 270 nm originates from the π-plasmon absorption of graphene.²⁹ The presence of these two peaks in the transferred sample clearly indicates the coexistence of graphene and h-BN. Moreover, the transparency for these samples can also be directly demonstrated by their photographs, as displayed in the inset of Fig. 3e. The h-BN domains exhibit extremely high transparency onto the quartz substrate, while the monolayer graphene and the graphene/h-BN hybrid film show almost identical characteristics.

We further characterized the in-plane graphene/h-BN heterostructures on Cu foils by XPS for elemental analysis, and the corresponding results are shown in Fig. 3f–h. The B 1s, N 1s and C 1s core-level peaks are centered at about 190.7, 398.2 and 284.8 eV, respectively, consistent with the values reported for bulk BN (190.1 eV and 398.1 eV) and graphene (284.9 eV).^{2,30} The B/N atomic ratio calculated from our XPS survey is

about 1.05 : 1, which is close to the 1 : 1 stoichiometry in h-BN. These results provide additional support for the growth of in-plane graphene/h-BN heterostructures.

The above investigations demonstrate that the large-area in-plane graphene/h-BN heterostructures and the graphene/h-BN hybrid film can be synthesized by controlling the growth time of CVD graphene on the IBSD-grown h-BN domains. Next, we carried out the synthesis of vertically stacked graphene/h-BN heterostructures by the direct growth of graphene on a continuous h-BN film. To investigate the effect of the layer number of h-BN on the growth of graphene, an h-BN film with both monolayer and bilayer (labelled as sub-bilayered h-BN) was used as the substrate. Fig. 4a shows a typical SEM image of the sub-bilayered h-BN film. A continuous monolayered h-BN film is generally featured with a large number of grain

boundaries (Fig. S4†). In contrast, apart from the h-BN grain boundaries indicated by the white arrows in Fig. 4a, many triangular h-BN domains with the lighter colour on the top layer (as indicated by the white dashed lines) can also be clearly observed, demonstrating the sub-bilayered nature of the h-BN film. After 3 min CVD growth, the h-BN grain boundaries disappeared, probably due to the H₂ etching effect. Interestingly, graphene with the darker colour only emerged from the gap between the top h-BN bilayers (Fig. 4b), revealing the preferential nucleation of graphene on the monolayered h-BN. The SEM and optical images (Fig. 4c and d) show that a uniform and continuous graphene film was grown on the sub-bilayered h-BN/Cu substrate by further increasing the growth time to 12 min, implying that a vertically stacked graphene/h-BN heterostructure was obtained. Some SiO₂ regions, as indicated by the white arrow in Fig. 4d, are visible after an intended scratch to bare and show the graphene/h-BN regions clearly.

HRTEM was used to examine the microstructure of the stacked graphene/h-BN film transferred onto TEM grids. As shown in Fig. 4e, a clear hexagonal Moiré pattern with a periodicity of 2.15 nm is observed in the HRTEM image, and the corresponding fast Fourier transform pattern for this region displays two sets of hexagonal spots with a rotational angle of 6° that arose from two rotated layers (inset of Fig. 4e). Since the lattice distance of graphene (0.2456 nm) is slightly smaller than that of h-BN (0.2504 nm), the set of the hexagonal spots with a smaller reciprocal lattice distance belongs to the h-BN lattice, while the other one comes from the graphene lattice.³¹ Therefore, the observed region in Fig. 4e captures the stacking region of a monolayer graphene that spreads on top of a monolayered h-BN (another example is shown in Fig. S5a†). In addition, a monolayer graphene on top of a bilayered h-BN can also be seen in the other region, as shown in Fig. S5b.†

To provide additional evidence on the layered structure of the sample, the 12 min grown graphene/h-BN film on Cu was characterized by angle-resolved XPS measurements, which is a surface-sensitive technique for non-destructive depth profile analysis. Fig. 4f shows the emission angle dependence of the atomic concentrations of elements from the as-grown graphene/h-BN on Cu, while all the raw XPS data are given in Fig. S6.† As expected, the atomic concentration of Cu appears to decrease with increasing emission angle (the angle between the substrate normal and the emission direction of the photoelectrons), while the signal of C from graphene monotonically increases with the angle. Interestingly, the concentration of N atoms rises gradually at the small emission angles; however, it starts to decrease when the emission angle is greater than 70°. These results suggest that graphene is the outermost atomic layer of the sample, matching well with the construction of vertically stacked graphene-on-h-BN.

Raman and UV-Vis absorption spectroscopies were also used to provide further information on the structure and quality of samples. Fig. 5a shows the Raman spectra for the graphene grown on the same sub-bilayered h-BN/Cu substrate with the growth time ranging from 3 to 12 min, and all of

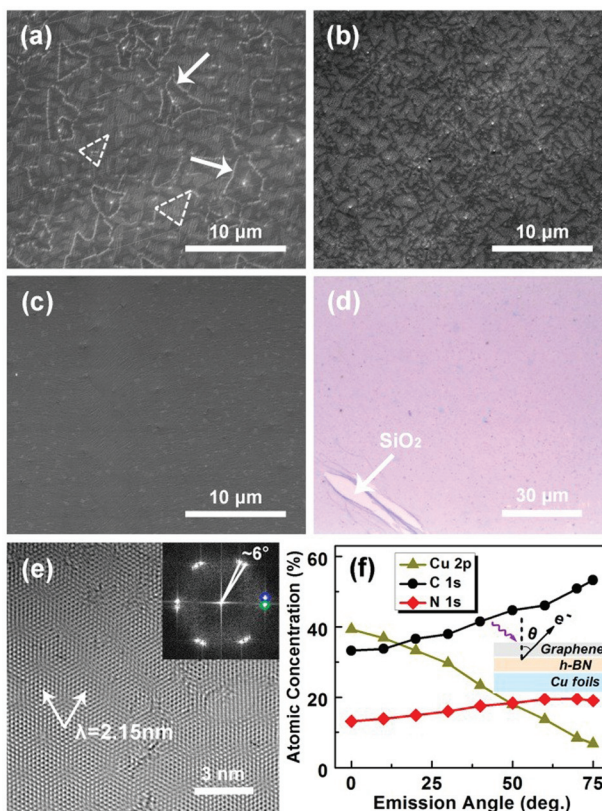


Fig. 4 Characterization of stacked graphene/h-BN heterostructures. (a) SEM image of the sub-bilayered h-BN film. The triangular h-BN domains with the lighter colour on the top layer are indicated by the white dashed lines, and the white arrows show the h-BN grain boundaries. (b, c) SEM images of graphene grown on the sub-bilayered h-BN film with the growth times of (b) 3 and (c) 12 min. (d) Optical micrograph of 12 min grown sample transferred onto a SiO₂/Si substrate. (e) HRTEM image of the stacked graphene/h-BN film showing the Moiré pattern of the 2.15 nm period. The inset in (e) shows the corresponding fast Fourier transform pattern, and two separate spots with a rotation angle about 6° can be recognized, one from h-BN and the other from graphene. (f) The emission angle dependence of the atomic concentrations of elements from the 12 min-grown graphene/h-BN on Cu, as determined from angle-resolved XPS measurements.

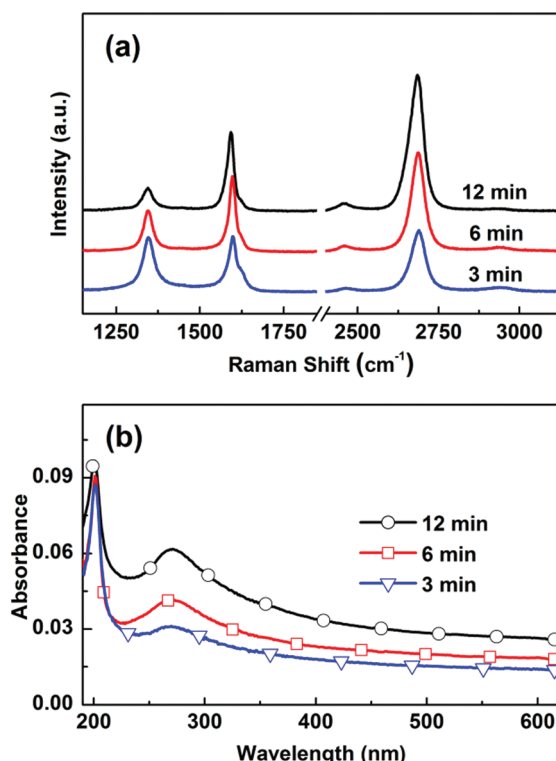


Fig. 5 (a) Raman spectra and (b) UV-Vis absorption spectra for the graphene grown on the same sub-bilayered h-BN/Cu substrate with the growth times of 3, 6 and 12 min.

them reveal the well known D, G and 2D peaks from graphene. It is noted that the intensity of the D peak gradually decreases with increasing the growth time, indicating that the defects are reduced when a continuous graphene layer was grown on h-BN. The smaller sizes of graphene grains result in a large amount of grain boundaries during the initial growth stage,

which is responsible for the higher intensity of the D peak.²² On the other hand, the intensity of the G peak almost maintains a constant, while that of the 2D peak gradually increases with the growth time, consequently, the peak intensity ratio $I_{2\text{D}}/I_{\text{G}}$ decreases from 1.71 at 12 min to 1.09 at 3 min. It was reported that the intensity ratio $I_{2\text{D}}/I_{\text{G}}$ is sensitive to not only the number of graphene layers but also the defect density.^{32,33} Combined with the D peak evolution with the growth time, we propose that a higher defect density in the sample with a shorter growth time is responsible for the decreased intensity of the 2D peak. Therefore, it can be concluded that the mono-layer graphene flakes or films were formed within these stacked graphene/h-BN heterostructures with various growth times.

As shown in Fig. 5b, the corresponding UV-Vis absorption spectra of these samples exhibit two characteristic absorption peaks at 200 and 270 nm, which originate from h-BN and graphene, respectively. The most important feature in Fig. 5b is that the overall intensity of absorption is remarkably enhanced with the increase of the growth time. As we all know, the UV-Vis absorption spectrum has been widely employed to determine the layer number of graphene by assuming an optical absorption of 2.3% for a monolayer graphene.^{29,34} Nevertheless, in our case, the difference in absorption between these samples is dominated by the different coverage of graphene rather than the change in thickness.

The above results indicate that the in-plane and stacked graphene/h-BN heterostructures can be synthesized by depositing graphene on the h-BN domains and the continuous h-BN films, respectively. Fig. 6 illustrates a schematic of the growth progression for graphene/h-BN heterostructures on both substrates. For the first route, the Cu foil substrates are partly covered by the h-BN domains, and thus graphene preferentially nucleates on the Cu foils due to the much weaker catalytic activity of h-BN than Cu. It was reported that the growth rate of graphene on a dielectric substrate was three to four

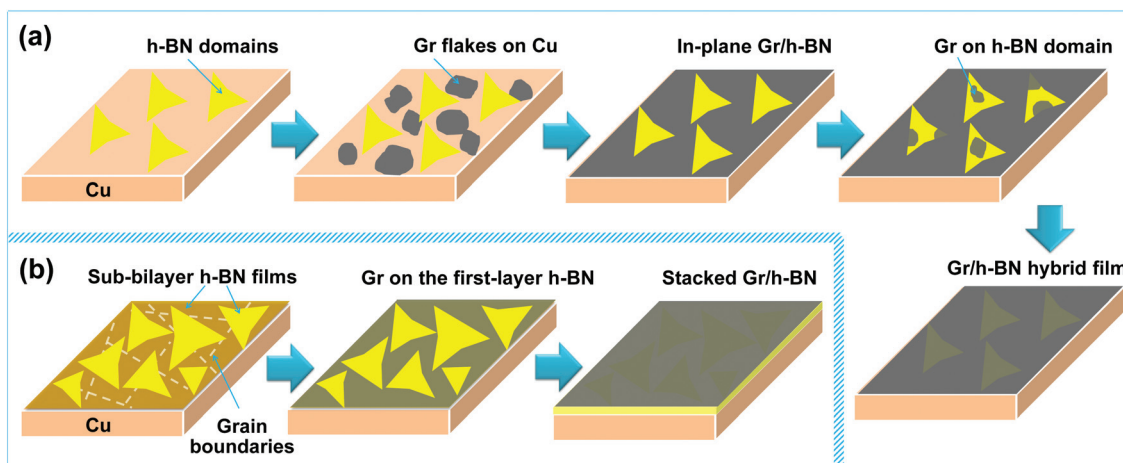


Fig. 6 Schematic illustration of the growth progression for the (a) in-plane and (b) stacked graphene/h-BN heterostructures on the h-BN domain and sub-bilayered h-BN substrates.

orders of magnitude slower than that obtained by CVD on a catalytic metal surface.¹⁸ The dramatic difference in the growth rate leads to the formation of in-plane graphene/h-BN heterostructure within a short growth time of 30 s. With the increase of the growth time, the graphene on Cu extends to the top of the nearby h-BN domains. Meanwhile, graphene can also nucleate directly on the h-BN domains owing to the catalytic transparency of h-BN on Cu.³⁵ Finally, the growing graphene grains were in contact with the adjacent grains and merged into a continuous layer, forming a graphene/h-BN hybrid film. For the second route, a sub-bilayered h-BN film is used as the substrate, and it is found that the graphene preferentially nucleates on the monolayered h-BN film. The same growth conditions except for the substrate provide convincing evidence that the monolayered h-BN on Cu exhibits higher catalytic activity than the bilayered h-BN on Cu. Similar to the first route, by further increasing the growth time, the graphene grows on the bilayered h-BN flakes and finally coalesces into a continuous film, resulting in a stacked graphene/h-BN heterostructure. An obvious difference between these two routes is the growth time for forming a continuous graphene film, and it is 90 s and 12 min for the growth on the h-BN domains and the sub-bilayered h-BN film, respectively. Again, the lower growth rate is attributed to the weaker catalytic activity of h-BN with the higher thickness, in which the charge transfer through h-BN from Cu is essential to the catalytic properties of the h-BN film surface.³⁵

Conclusions

In summary, we have demonstrated a new method for the synthesis of both in-plane and stacked graphene/h-BN heterostructures by sequentially depositing h-BN via IBSD and graphene with CVD. It was found that graphene preferentially nucleated on the Cu foils rather than the h-BN domains due to the weak catalytic activity of h-BN, leading to the formation of in-plane graphene/h-BN heterostructures. The large-area vertically stacked graphene/h-BN heterostructures were obtained by using the continuous h-BN film as a substrate. Furthermore, the well-designed sub-bilayered h-BN substrates provide direct evidence that the monolayered h-BN on Cu exhibits higher catalytic activity than the bilayered h-BN on Cu. The growth method applied here may have great potential in the scalable preparation of large-area high-quality graphene/h-BN heterostructures.

Acknowledgements

This work was financially supported by the National Natural Science Foundation of China (No. 61376007), the National Basic Research Program of China (No. 2012CB619306), and the Beijing Natural Science Foundation (No. 2142032).

Notes and references

- H. Wang, F. C. Liu, W. Fu, Z. Y. Fang, W. Zhou and Z. Liu, *Nanoscale*, 2014, **6**, 12250–12272.
- L. Song, L. J. Ci, H. Lu, P. B. Sorokin, C. H. Jin, J. Ni, A. G. Kvashnin, D. G. Kvashnin, J. Lou, B. I. Yakobson and P. M. Ajayan, *Nano Lett.*, 2010, **10**, 3209–3215.
- K. K. Kim, A. Hsu, X. T. Jia, S. M. Kim, Y. M. Shi, M. Hofmann, D. Nezich, J. F. Rodriguez-Nieva, M. Dresselhaus, T. Palacios and J. Kong, *Nano Lett.*, 2012, **12**, 161–166.
- K. H. Lee, H.-J. Shin, J. Lee, I.-Y. Lee, G.-H. Kim, J.-Y. Choi and S.-W. Kim, *Nano Lett.*, 2012, **12**, 714–718.
- K. K. Kim, A. Hsu, X. T. Jia, S. M. Kim, Y. M. Shi, M. Dresselhaus, T. Palacios and J. Kong, *ACS Nano*, 2012, **6**, 8583–8590.
- C. H. Zhang, S. L. Zhao, C. H. Jin, A. L. Koh, Y. Zhou, W. G. Xu, Q. C. Li, Q. H. Xiong, H. L. Peng and Z. F. Liu, *Nat. Commun.*, 2015, **6**, 6519.
- L. J. Ci, L. Song, C. H. Jin, D. Jariwala, D. X. Wu, Y. J. Li, A. Srivastava, Z. F. Wang, K. Storr, L. Balicas, F. Liu and P. M. Ajayan, *Nat. Mater.*, 2010, **9**, 430–435.
- X. F. Fan, Z. X. Shen, A. Q. Liu and J.-L. Kuo, *Nanoscale*, 2012, **4**, 2157–2165.
- C.-K. Chang, S. Kataria, C.-C. Kuo, A. Ganguly, B.-Y. Wang, J.-Y. Hwang, K.-J. Huang, W.-H. Yang, S.-B. Wang, C.-H. Chuang, M. Chen, C.-I. Huang, W.-F. Pong, K.-J. Song, S.-J. Chang, J.-H. Guo, Y. Tai, M. Tsujimoto, S. Isoda, C.-W. Chen, L.-C. Chen and K.-H. Chen, *ACS Nano*, 2013, **7**, 1333–1341.
- C. R. Dean, A. F. Young, I. Meric, C. Lee, L. Wang, S. Sorgenfrei, K. Watanabe, T. Taniguchi, P. Kim, K. L. Shepard and J. Hone, *Nat. Nanotechnol.*, 2010, **5**, 722–726.
- A. S. Mayorov, R. V. Gorbachev, S. V. Morozov, L. Britnell, R. Jalil, L. A. Ponomarenko, P. Blake, K. S. Novoselov, K. Watanabe, T. Taniguchi and A. K. Geim, *Nano Lett.*, 2011, **11**, 2396–2399.
- C. R. Dean, L. Wang, P. Maher, C. Forsythe, F. Ghahari, Y. Gao, J. Katoh, M. Ishigami, P. Moon, M. Koshino, T. Taniguchi, K. Watanabe, K. L. Shepard, J. Hone and P. Kim, *Nature*, 2013, **497**, 598–602.
- W. Yang, G. R. Chen, Z. W. Shi, C. C. Liu, L. C. Zhang, G. B. Xie, M. Cheng, D. M. Wang, R. Yang, D. X. Shi, K. Watanabe, T. Taniguchi, Y. G. Yao, Y. B. Zhang and G. Y. Zhang, *Nat. Mater.*, 2013, **12**, 792–797.
- M. P. Levendorf, C.-J. Kim, L. Brown, P. Y. Huang, R. W. Havener, D. A. Muller and J. Park, *Nature*, 2012, **488**, 627–632.
- Z. Liu, L. L. Ma, G. Shi, W. Zhou, Y. J. Gong, S. D. Lei, X. B. Yang, J. N. Zhang, J. J. Yu, K. P. Hackenberg, A. Babakhani, J.-C. Idrobo, R. Vajtai, J. Lou and P. M. Ajayan, *Nat. Nanotechnol.*, 2013, **8**, 119–124.
- G. H. Han, J. A. Rodríguez-Manzo, C.-W. Lee, N. J. Kybert, M. B. Lerner, Z. J. Qi, E. N. Dattoli, A. M. Rappe, M. Drndic and A. T. C. Johnson, *ACS Nano*, 2013, **7**, 10129–10138.

- 17 L. Liu, J. Park, D. A. Siegel, K. F. McCarty, K. W. Clark, W. Deng, L. Basile, J. C. Idrobo, A.-P. Li and G. Gu, *Science*, 2014, **343**, 163–167.
- 18 S. J. Tang, H. M. Wang, H. S. Wang, Q. J. Sun, X. Y. Zhang, C. X. Cong, H. Xie, X. Y. Liu, X. H. Zhou, F. Q. Huang, X. S. Chen, T. Yu, F. Ding, X. M. Xie and M. H. Jiang, *Nat. Commun.*, 2015, **6**, 6499.
- 19 Z. Liu, L. Song, S. Z. Zhao, J. Q. Huang, L. L. Ma, J. N. Zhang, J. Lou and P. M. Ajayan, *Nano Lett.*, 2011, **11**, 2032–2037.
- 20 M. Wang, S. K. Jang, W.-J. Jang, M. Kim, S.-Y. Park, S.-W. Kim, S.-J. Kahng, J.-Y. Choi, R. S. Ruoff, Y. J. Song and S. Lee, *Adv. Mater.*, 2013, **25**, 2746–2752.
- 21 S. M. Kim, A. Hsu, P. T. Araujo, Y. H. Lee, T. Palacios, M. Dresselhaus, J.-C. Idrobo, K. K. Kim and J. Kong, *Nano Lett.*, 2013, **13**, 933–941.
- 22 T. Gao, X. J. Song, H. W. Du, Y. F. Nie, Y. B. Chen, Q. Q. Ji, J. Y. Sun, Y. L. Yang, Y. F. Zhang and Z. F. Liu, *Nat. Commun.*, 2015, **6**, 6835.
- 23 H. L. Wang, X. W. Zhang, J. H. Meng, Z. G. Yin, X. Liu, Y. J. Zhao and L. Q. Zhang, *Small*, 2015, **11**, 1542–1547.
- 24 P. Sutter, J. Lahiri, P. Albrecht and E. Sutter, *ACS Nano*, 2011, **5**, 7303–7309.
- 25 Y. A. Wu, Y. Fan, S. Speller, G. L. Creeth, J. T. Sadowski, K. He, A. W. Robertson, C. S. Allen and J. H. Warner, *ACS Nano*, 2012, **6**, 5010–5017.
- 26 D. C. Geng, B. Wu, Y. L. Guo, L. P. Huang, Y. Z. Xue, J. Y. Chen, G. Yu, L. Jiang, W. P. Hu and Y. Q. Liu, *Proc. Natl. Acad. Sci. U. S. A.*, 2012, **109**, 7992–7996.
- 27 Y. Miyata, E. Maeda, K. Kamon, R. Kitaura, Y. Sasaki, S. Suzuki and H. Shinohara, *Appl. Phys. Express*, 2012, **5**, 085102.
- 28 R. V. Gorbachev, I. Riaz, R. R. Nair, R. Jalil, L. Britnell, B. D. Belle, E. W. Hill, K. S. Novoselov, K. Watanabe, T. Taniguchi, A. K. Geim and P. Blake, *Small*, 2011, **7**, 465–468.
- 29 R. R. Nair, P. Blake, A. N. Grigorenko, K. S. Novoselov, T. J. Booth, T. Stauber, N. M. R. Peres and A. K. Geim, *Science*, 2008, **320**, 1308–1308.
- 30 Z. Z. Sun, Z. Yan, J. Yao, E. Beitzler, Y. Zhu and J. M. Tour, *Nature*, 2010, **468**, 549–552.
- 31 M. Yankowitz, J. M. Xue, D. Cormode, J. D. Sanchez-Yamagishi, K. Watanabe, T. Taniguchi, P. Jarillo-Herrero, P. Jacquod and B. J. LeRoy, *Nat. Phys.*, 2012, **8**, 382–386.
- 32 I. Childres, L. A. Jauregui, J. Tian and Y. P. Chen, *New J. Phys.*, 2011, **13**, 025008.
- 33 L. G. Cançado, A. Jorio, E. H. M. Ferreira, F. Stavale, C. A. Achete, R. B. Capaz, M. V. O. Moutinho, A. Lombardo, T. S. Kulmala and A. C. Ferrari, *Nano Lett.*, 2011, **11**, 3190–3196.
- 34 S. Bae, H. Kim, Y. Lee, X. F. Xu, J.-S. Park, Y. Zheng, J. Balakrishnan, T. Lei, H. R. Kim, Y. I. Song, Y.-J. Kim, K. S. Kim, B. Özylmaz, J.-H. Ahn, B. H. Hong and S. Iijima, *Nat. Nanotechnol.*, 2010, **5**, 574–578.
- 35 M. Wang, M. Kim, D. Odkhuu, N. Park, J. Lee, W.-J. Jang, S.-J. Kahng, R. S. Ruoff, Y. J. Song and S. Lee, *ACS Nano*, 2014, **8**, 5478–5483.